Int. J. Electrochem. Sci., 16 **(2021)** Article ID: 210618, doi: 10.20964/2021.06.11

International Journal of
ELECTROCHEMICAL
SCIENCE
www.electrochemsci.org

Fabrication of $TiO_2@FeS_2$ Nanocomposite for Photocatalytic Degradation of Organic Dyes in the Industrial Wastewater

Bangjun Han, Xingya Wei, Renzheng Gu[*]

School of Civil and Transportation Engineering, Shanghai Urban Construction Vocational College,
200438 Shanghai, P. R. China
[*]E-mail: gurenzheng@succ.edu.cn

Received: 3 Febuary 2021 / *Accepted:* 16 March 2021 / *Published:* 30 April 2021

This study was conducted on synthesis of titanium dioxide (TiO_2) and Iron disulfide (FeS_2) nanocomposite ($TiO_2@FeS_2$ NC) as a photocatalyst for degradation of methyl orange (MO) as chemical pollutants in the industrial wastewater. The TiO_2, FeS_2 and $TiO_2@FeS_2$ NC were synthesized through chemical methods. The morphology and crystal structure of prepared samples were studied using FESEM and XRD analyses. The results showed humongous mixture of TiO_2 and FeS_2 in $TiO_2@FeS_2$ NC. Optical study revealed that the band-gap values for TiO_2, FeS_2 and $TiO_2@FeS_2$ NC films were obtained 3.07, 2.74, and 2.88 eV, respectively. Electrochemical characterization exhibited that specific capacitance of $TiO_2@FeS_2$ NC was more than TiO_2 and FeS_2 due to effective incorporation Ti and Fe ions to nanocomposite structure and higher effective surface area. The results of photodegradation studies showed the complete degradation of 20 mg/l of MO in the presence of $TiO_2@FeS_2$ NC photocatalyst were achieved under 65 and 58 minutes UV and visible light irradiations, respectively. Results showed that the degradation efficiency of TiO_2 film was significantly improved 20% and 33% by mixing FeS_2 in $TiO_2@FeS_2$ NC under UV and visible irradiation, respectively.

Keywords: Photocatalytic degradation; Methyl orange; TiO_2 and FeS_2 nanocomposite; Band gap; Degradation efficiency

1. INTRODUCTION

Organic dyes pollutants from the industrial wastewater sources such as textile, paper, leather, pulp, soap, plastic, chemical, petrochemical, ink, palm oil can be released in the natural ecosystem and contaminate the underground water sources, agricultural soils, lake and river [1, 2]. Studies confirmed that some industrial organic dyes are exceeding toxic and show great hazard to the natural environment due to their aromatic amine toxicity [3]. Today, industrial development and improper waste management lead to increased organic dyes pollutants in habitat of humans and animals and creates significant health problems and carcinogenic effects [4, 5].

The more applicant industrial organic dyes contains methyl orange, methyl red, rhodamine B, alizarin S, methylene blue, congo red, and acid chrome blue k. among them, methyl orange (MO, Benzenesulfonic acid, p-((p-(dimethylamino)phenyl) azo)-, sodium salt) is one of most frequently azo dyes in medical and chemical labs and the printing, pharmaceutical, and textiles industries. Accordingly, many studies have been conducted on development identify and degradation techniques of MO in environment and industrial wastewater [6-8]. The degradation techniques of MO include coagulation, adsorption, flocculation, ozonation, ion exchange, reverse osmosis, electro-osmosis and photocatalytic degradation. Many studies have been performed using photocatalytic degradation for to remove the organic dyes pollutants from the industrial wastewater because of inexpensiveness, high efficiency, simplicity and excellent stability of photodegradation process with irritation light sources in presence of nontoxic semiconductors such as TiO_2, SiO_2, CuO,Fe_2O_3,SnO_2,ZnO, Al_2O_3, etc[9-13].

Furthermore, modification of the photocatalyst materials and morphology of electrode surfaces with doping, hybrid and composite materials and nanostructures can change the optical and electronic structure of electrodes, and consequently improve the photodegradation rate [14-19]. For example, Gonget al. [10] synthesized Ru-doped TiO_2 Nanostructured as photocatalyst to photodegradation the MO under visible and UV irradiations. Their results indicated that the removal rate was enhanced through Ru doping and the whole degradation of MO after 45 and 55 minutes irradiation of sunlight and UV, respectively. Tan et al. [15] synthesized V_2O_5@ZnO nanocomposite as a photocatalyst for degradation of MO. They showed a combination of V_2O_5 nanoparticles in ZnO nanorods structure led to narrowing the band-gap of nanocomposite toward the ZnO film which improved degradation of MO under visible light irradiation.

Although many studies had been carried out to investigate photocatalytic properties of semiconductor materials, the TiO_2@FeS_2 nanocomposites have never been evaluated before. Therefore, this study was conducted on fabrication TiO_2@FeS_2 nanocomposite for photocatalytic degradation of MO as organic dyes in the industrial wastewater.

2. EXPERIMENTAL

In order to preparation of TiO_2@FeS_2NC, the mixture of 4 g of $FeSO_4$ (98%, Shandong Kaiteda Chemical Co., Ltd., China), 9 g of $Na_2S_2O_3.5H_2O$(98%, Qingdao HiseaChem Co., China) and 4g $TiCl_4$ (99.9%, Hebei Yanxi Chemical Co., China) were ultrasonically added in 200 ml of ethanol (96%, Shandong Kawah Oils Co., Ltd., China) for 120 minutes at 160 °C.The obtained suspension was filtered (3 µm, Guangzhou Lvyuan Water Purification Equipment Co., Ltd., China) and rinsed with deionized water. The filtered suspension was washed with acetone and dried at 75 °C for 14 hours.

Scanning electron microscopy (SEM, Zeiss Supra 40VP) was used to characterize morphology of synthesized samples. The crystal structures were studied by X-ray diffraction (XRD, X'Pert MPD, Philips, Holand). In order electrochemical study, cyclic voltammetry (CV) measurements were conducted on potentiostat (PGSTAT128N, Metrohm Autolab B.V., Utrecht, The Netherlands) in a standard three-electrode electrochemical cell which contained Ag/AgCl electrode as the reference electrode, Pt plate as the counter electrode and the prepared samples (TiO_2, FeS_2 and TiO_2@FeS_2 NC) as working electrode. The electrolyte of CV measurement was 0.1 M KOH (95%, Shandong Kaiteda Chemical Co., Ltd., China) solutions.

Photodegradation measurements were performed in a test chamber which contained a photocatalyst (TiO_2, FeS_2 and $TiO_2@FeS_2$ NC) and the 20 mg/l of methyl orange (99.5%, Lonwin Industry Group Limited., China) aquatic solution. Optical absorption spectra of synthesized films were done by a UV-VIS spectrophotometer (Perkin-Elmer, 550ES spectrometer, MA, USA). 300 W Xe Lamp (Shandong Gelon Lib Co., Ltd., China) and UV Lamp (365nm, TaoYuan Optoelectronics Shenzhen Co., Ltd., China) were employed to irradiate the visible and UV lights, respectively. Optical absorption spectra was recorded after lights irradiations and the degradation efficiency was measured using recorded absorption intensity of degraded dye according to following equation[15]:

$$\text{Degradation efficiency (\%)} = (1 - \frac{I_t}{I_0}) \times 100 = (1 - \frac{C_t}{C_0}) \times 100 \qquad (1)$$

Where, C_0 and I_0 are concentration and absorption intensity of undegraded MO solution, respectively. I_t and C_t are absorption intensity and concentration of irradiated MO solution, respectively.

The efficiency of the prepared photocatalyst was also evaluated on a wastewater effluent sampled from municipal sewage and industrial wastewater of Shanghai, China. The sample was filtered and centrifuged at 1500 rpm, and supernatant was used as a real sample to prepare the 5 mg/l MO solution.

3. RESULTS AND DISCUSSION

SEM images in Figure 1 shows the surface morphologies of the TiO_2, FeS_2 and $TiO_2@FeS_2$ NC electrodes. As observed from Figure 1a, there are a large number of TiO_2 nanorods with average diameter about 100 nm. The morphology of FeS_2 film in Figure 1b shows the cubic-shape structures with average side length of 70 nm. Figure 1c displays the SEM of $TiO_2@FeS_2$ NC with a bunch of rods and rod-like structures with average diameter about 110 nm.

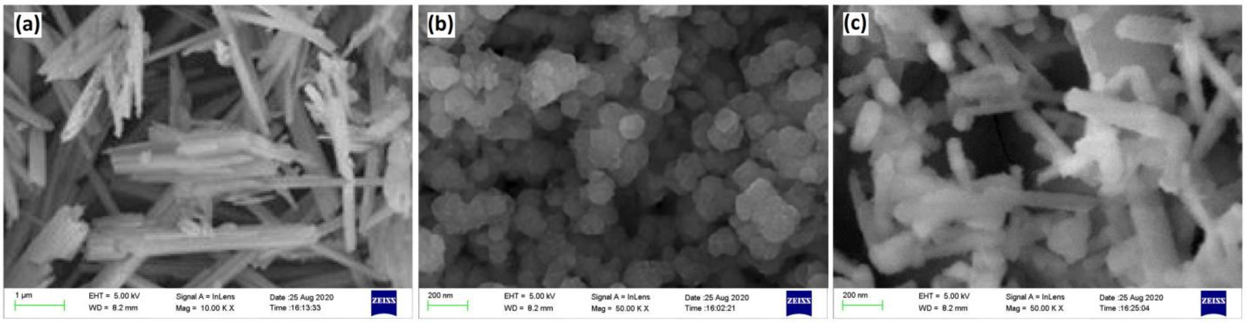

Figure 1. SEM images of the (a) TiO_2, (b) FeS_2 and (c) $TiO_2@FeS_2$NC films.

XRD patterns of TiO_2, FeS_2 and $TiO_2@FeS_2$ NC are shown in Figure 2a to 2c. XRD pattern of the TiO_2 in Figure 2a shows recorded diffraction peaks at 2θ = 25.75°, 38.03°, 48.01°,54.48°, 62.78°, 69.03° and 75.22° can be attributed to the (101), (004), (200), (105), (213), (204), (116), and (215) crystalline planes, respectively, which demonstrated to anatase crystal structure TiO_2 (JCPDS card No.21-1272)[20]. The XRD patterns of FeS_2 (Figure 2b) exhibits diffracted peaks at 2θ = 28.25°, 32.93°, 36.68°, 40.53°, 46.98°, 56.14°, 58.74°, 61.34° and 63.82° can be associated with (111), (200), (210), (211), (220), (311), (222), (023) and (321) crystalline planes, respectively, which reflected to cubic pyrite crystal structure of FeS_2 (JCPDS card No. 42-1340)[21]. For TiO_2@FeS_2 NC sample, XRD pattern shows all diffraction peaks of TiO_2 and some diffraction peaks related to (200), (210), (211), (311), (222) and (023) crystalline planes of crystal structure of FeS_2 which signified to good mixture of TiO_2 and FeS_2 in nanocomposite.

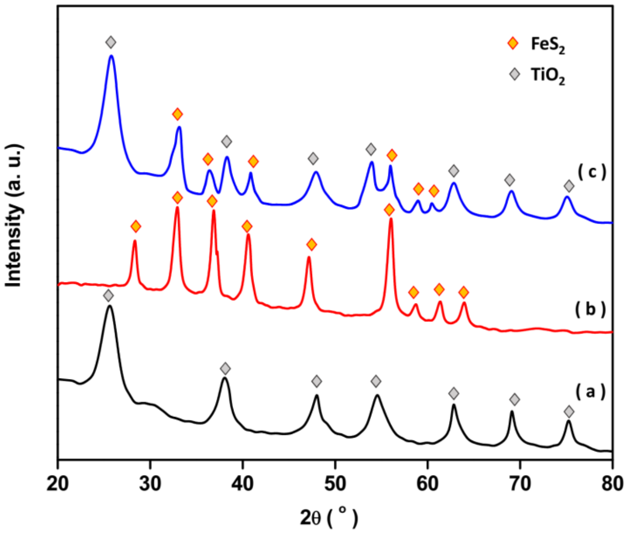

Figure 2. XRD pattern of (a) TiO_2, (b) FeS_2 and (c) TiO_2@FeS_2 NC films

Optical property of TiO_2, FeS_2 and TiO_2@FeS_2 NC films was investigated through UV-Vis spectra. The recorded absorption spectra are shown in Figure 3a. Figure 3a indicates the absorption of Ti_4^{+}in wavelength from 350 to 380 nm for synthesized TiO_2 film and associated with the transitions from the TiO_2 valence band from the oxygen vacancies to the TiO_2 conduction band [22]. The absorption spectra of FeS_2 exhibited the absorbance in 340 to 380nm. Absorption spectra of TiO_2@FeS_2 NC film shows the spectra similar to spectra of TiO_2 film with wider absorption wavelength range (350 to 390 nm). The tail broadening of absorption peak in composite can be related to the presence of a sulfur component [23]. The absorption of TiO_2@FeS_2 NC film is obtained from UV to NIR due to the combination of the absorption spectra of TiO_2 and FeS_2 films [24]. Therefore, the absorption spectra of TiO_2@FeS_2 NC film is developed from UV to NIR compared to that of TiO_2 film. Figure 3 shows Tauc plot of TiO_2 and TiO_2@FeS_2 NC films that calculated using equation (2) and by extrapolation of the linear portion of higher photon energy to zero absorption coefficient (α=0) [25]:

$$(\alpha h\nu)^{1/2} = A\,(h\nu - E_g) \qquad (2)$$

Where α is the absorption coefficient of the semiconductor, Eg is the optical band gap energy, A is a proportionality constant, hν is the energy of the photon. As observed, the band gap values in a synthesized semiconductor are closely correlated to absorbed wavelength. The obtained band gap values for TiO_2, FeS_2 and TiO_2@FeS_2 NC films are 3.07, 2.74, and 2.88 eV, respectively. In addition, the band gap values are decreased by increasing absorption wavelength. The semiconductor with a wide band gap can be applied as photoactive materials for the UV region [26]. The narrow band gap films can be used for visible light. This is important because the semiconductor with very small band gap (<2.8 eV) shows very poor photo-activity because of higher rate of electron-hole recombination [27].

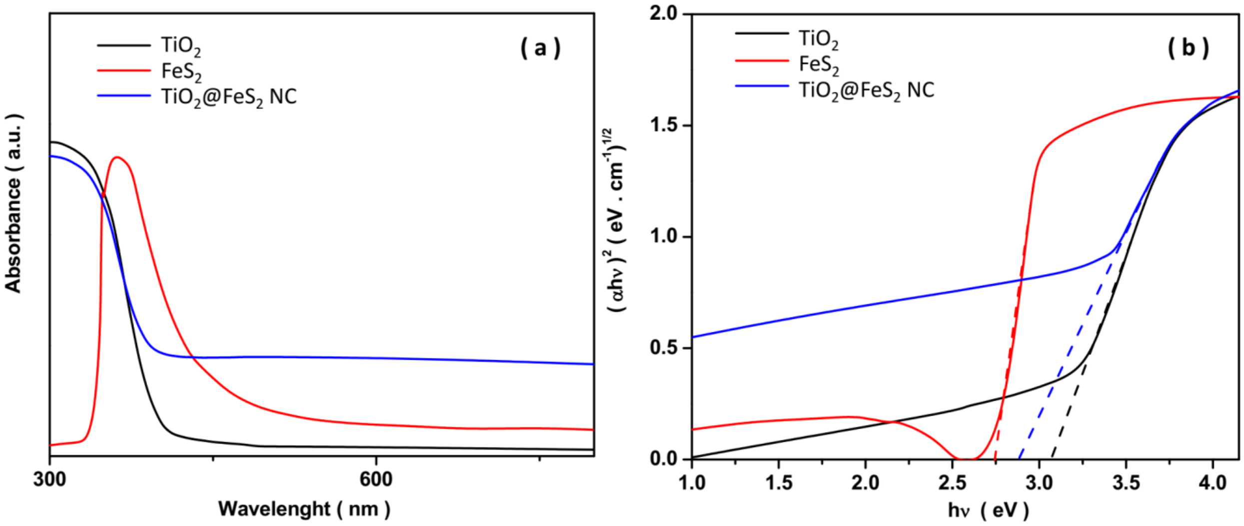

Figure 3. (a) UV-Vis absorption spectra and (b) calculation band gap energy of TiO_2, FeS_2 and TiO_2@FeS_2 NC films using Tauc plot method.

The electrochemical behaviour of TiO_2, FeS_2 and TiO_2@FeS_2 NC films were investigated by CV technique in 0.1 M KOH at scan rate of 20 mV/s. As shown in Figure 4a, the CV of TiO_2 film exhibits redox peaks at 0.06 V and 0.41 Vare attributed to the interconversion between Ti^{3+} and Ti^{4+} [28]. For FeS_2 film, the recorded CV in Figure 4b shows oxidation and reduction peaks at -0.14 V and 0.66 V which describe the interconversion between Fe^{2+} and Fe^{4+} [29]. The recorded CV of TiO_2@FeS_2 NC film displays the both redox peaks of TiO_2 and FeS_2 due to a pair of oxidation-reduction processes of Ti and Fe nanocomposite. In addition, TiO_2@FeS_2 NC film exhibits the larger area surrounded within the CV curve which illustrated to its specific capacitance enhancement than TiO_2 and FeS_2 due to effective incorporation Ti and Fe ions to nanocomposite structure and higher effective surface area [30]. The higher effective surface area can be related to the larger number of surface active sites and faster spatial charge transfer [31]. Studies have proved that as the specific surface area, charge-carrier dynamics and light absorption efficiency of photocatalysts also changed, and then the yield changed accordingly [32, 33].

Figure 5 and 6 display degradation efficiency of 20 mg/l of MO in the presence of TiO2, FeS_2 and TiO_2@FeS_2 NC photocatalysts and without photocatalyst under-dark, UV and visible irradiations. As indicated in Figure 5, degradation efficiencies of 0.07 %, 1.19 %, 1.07 % and 1.31 % are obtained after 30 minutes, and 0.12 %, 1.29 %, 1.21 % and 1.41 % are obtained after 150 minutes for blank, TiO_2, FeS_2 and TiO_2@FeS_2 NC photocatalysts under dark condition, respectively. Therefore, results for dark conditions show that the poor degradation (less than 1.5%) happens in the first 30minutes and degradation rate is insignificant for the last 120 minutes. Therefore, before the degradation measurements under UV and visible irradiations, the MO solutions were maintained for 35 minutes in darkness to achieve adsorption-desorption equilibrium.

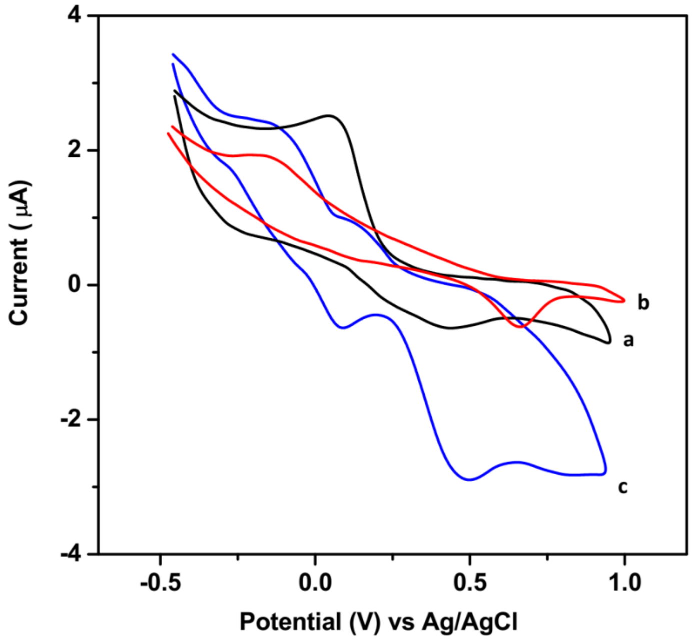

Figure 4. (a) The CV curves of (a) TiO_2, (b) FeS_2 and (c) TiO_2@FeS_2 NC films in 0.1 M KOH at scan rate of 20 Mv/s.

Furthermore, the MO degradation efficiencies are 1.39 %, 83.20%, 36.20 % and 100% for blank samples, TiO_2, FeS_2 and TiO_2@FeS_2 NC photocatalysts for 65 min UV radiation, respectively (Figure 6a). The complete degradation of MO for TiO_2 film is obtained after 100 minutes UV irradiation. Figure 6b exhibits the photodegradation efficiencies of 0.87 %, 75.71 %, 38.50 % and 100 % are obtained for blank sample, TiO_2, FeS_2 and TiO_2@FeS_2 NC photocatalysts for 60 minutes visible irradiation, respectively. Moreover, the complete degradation of MO is observed after 58 and 120 minutes visible irradiation at present of TiO_2@FeS_2 NC and TiO_2 photocatalysts, respectively. Accordingly, the degradation efficiency of TiO_2 film significantly is improved 20% and 33% by mixing FeS_2 in TiO_2@FeS_2 NC under UV and visible irradiation, respectively. The incorporation of FeS_2 can change in the TiO_2 electronic structure due to induce oxygen vacancies and creation of new energy levels inside the band gap of TiO_2 that make active $TiO_2@FeS_2$ NC under visible light irradiation [34, 35]. These new energy levels can improve the photoexcited electron-hole separation and promote the density of participated charges in the photodegradation of MO [36]. FeS_2 shows the minimum degradation rate in both UV and visible irradiations because of its narrow band gap it can be easily excited under visible light but its higher electron–hole recombination rate decreases degradation rate in visible light region [37]. These results are in agreement with the optical and electrochemical studies of this work.

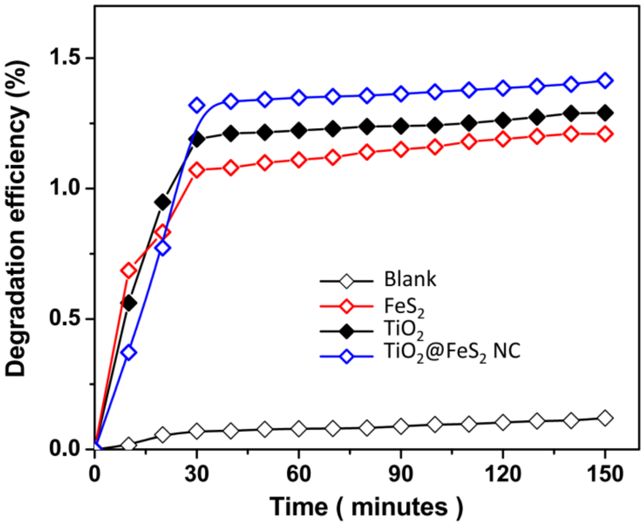

Figure 5. Degradation efficiency of 20 mg/l of MO in blank sample and present of TiO_2, FeS_2 and $TiO_2@FeS_2$ NC photocatalysts under dark condition

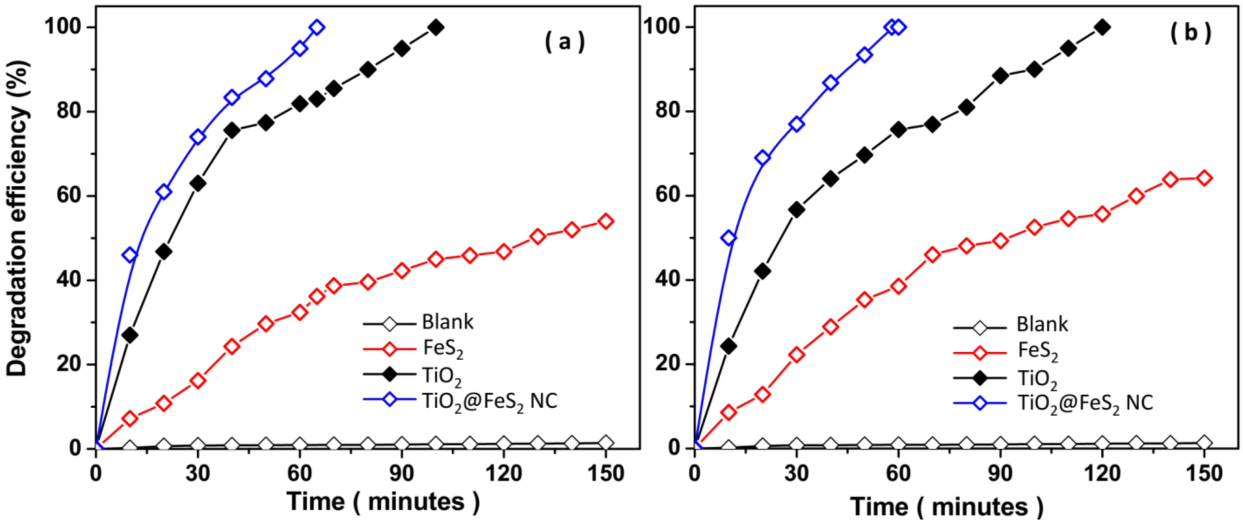

Figure 6. Degradation efficiency of 20 mg/l of MO in blank sample and present of TiO_2, FeS_2 and $TiO_2@FeS_2$ NC photocatalysts under (a) UV and (b) visible irradiations.

The obtained results of this work were compared with other based TiO_2 photocatalyst for degradation efficiency of MO in Table 1. The comparison reveals the great photocatalytic activity of TiO_2@FeS_2 NC to degradation of MO under visible light irradiation which attributed to the synergistic effect of the porosity which facilitates electron-transfer in the interface between TiO_2 and FeS_2, plentiful anatase and cubic pyrite interfaces, and oxygen vacancies can promote charge separation in the TiO_2@FeS_2 NC [38].

Table 1. Comparison between the obtained results of degradation efficiencies of MO in presents TiO_2, FeS_2 and TiO_2@FeS_2 NC photocatalysts with other TiO_2 based photocatalyst.

Material	**MO content (mg/l)**	**Source**	**Degradation time (minute)**	**Degradation efficiency (%)**	**Ref.**
TiO_2	20.00	UV visible	100 120	100 100	This work
FeS_2	20.00	UV visible	65 60	36.2 38.5	This work
TiO_2@FeS_2 NC	20.00	UV visible	65 58	100 100	This work
Fe-doped TiO_2porous microspheres	20.00	visible	360	70	[11]
Pt-doped TiO_2loaded on natural zeolite	20.00	UV	90	98	[12]
Cu-doped TiO_2 NPs	10.00	visible	45	100	[39]
N-doped TiO_2 NPs	20.00	visible	60	14	[40]
S-doped TiO_2 NPs	20.00	visible	100	98	[41]
Fe-doped TiO_2 NTs	20.00	UV-vis	180	99.7	[42]
Ru-doped TiO2 NRs	20.00	UV visible	55 45	100 100	[10]

Figure 7a and 7b show the UV–Vis spectra of photocatalytic degradation reaction of 5 mg/l MO prepared from deionized water as model solution and real sample with respect to different irradiation times by TiO_2@FeS_2 NC photocatalyst. It can be observed for both of samples that the intensity of the absorption peaks at 450 nm continuously decreases during the photodegradation reactions which similar to reported results of MO degradation over Fe_3O_4@SiO_2@TiO_2 microspheres [43]. The peak is disappeared after 15 and 20 minutes degradationin model solution and real sample, respectively. The degradation time for prepared solution with real sample is higher that the model solution due to presence of MO in background of wastewater. Therefore, the novelty of this study lies in facile and low-cost synthesis of TiO_2 based photocatalysis to treat MO from industrial wastewater under visible irradiation.

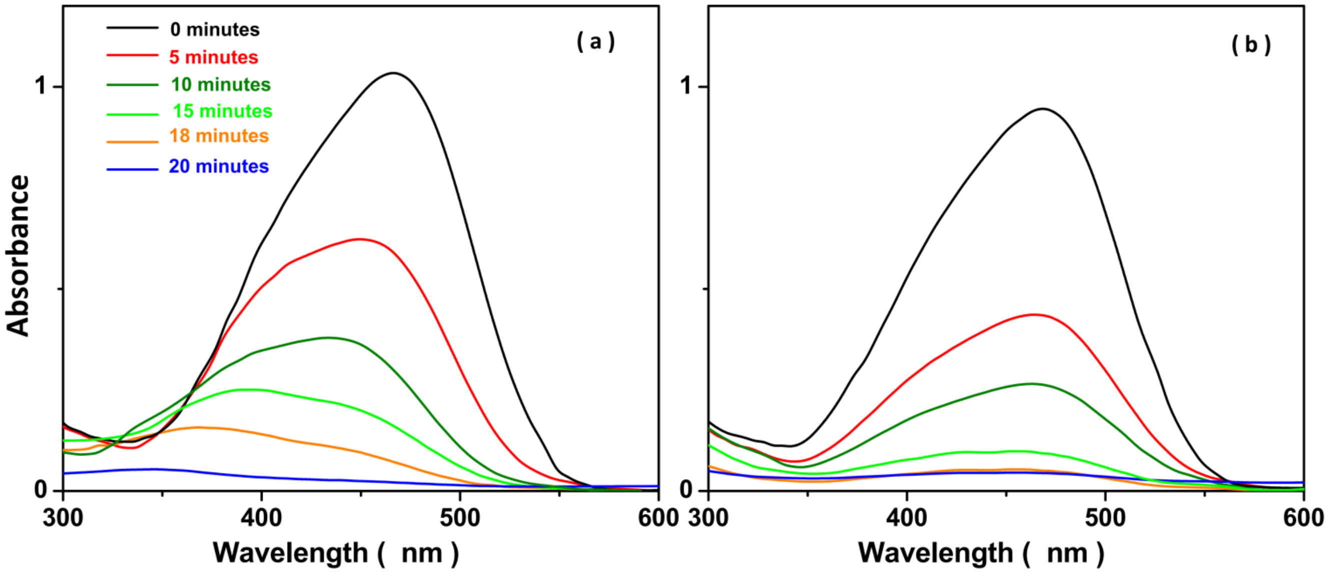

Figure 7. UV–Vis spectra of photocatalytic degradation reaction of 5 mg/l MO prepared from (a) deionized water as model solution and (b) real sample with respect to different irradiation times byTiO_2@FeS_2 NC photocatalyst.

4. CONCLUSION

This work was carried out to fabricate TiO_2@FeS_2NC for photocatalytic degradation of MO as organic dyes in the industrial wastewater. The TiO_2, $FeS_2$and TiO_2@FeS_2 NC were synthesized through chemical approach and the morphology and crystal structure of prepared samples were studied using FESEM and XRD analyses. The structural findings showed that humongous mixture of TiO_2 and FeS_2 in TiO_2@FeS_2 NC. Results of optical characterization showed that the band gap values for TiO_2, FeS_2 and TiO_2@FeS_2 NC films were obtained 3.07, 2.74, and 2.88 eV, respectively, and addition FeS_2 caused a narrowing band gap in composite film. Electrochemical study exhibited that specific capacitance of TiO_2@FeS_2 NC was more than TiO_2 and FeS_2 due to effective incorporation of Ti and Fe ions to nanocomposite structure and higher effective surface area. Photodegradation studies showed the complete degradation of 20 mg/l of MO in the presence of TiO_2@FeS_2 NC photocatalyst was achieved after 65 and 58 minutes UV and visible light irradiations, respectively. Results revealed that the degradation efficiency of TiO_2 film was significantly improved 33% and 20% by mixing FeS_2 in TiO_2@FeS_2 NC under visible and UV irradiation, respectively. The incorporation of FeS_2 can change in the TiO_2 electronic structure due to induce oxygen vacancies and creation of new energy levels inside the band-gap of TiO_2 that make active TiO_2@FeS_2 NC under visible light irradiation. These new energy levels can improve the photoexcited electron-hole separation and promote the density of participating charges in the photodegradation of MO.

References

1. E.T. Helmy, A. El Nemr, M. Mousa, E. Arafa and S. Eldafrawy, *Journal of Water and Environmental Nanotechnology*, 3 (2018) 116.
2. H. Karimi-Maleh, Y. Orooji, A. Ayati, S. Qanbari, B. Tanhaei, F. Karimi, M. Alizadeh, J. Rouhi, L. Fu and M. Sillanpää, *Journal of Molecular Liquids*, 329 (2021) 115062.
3. B. Lellis, C.Z. Fávaro-Polonio, J.A. Pamphile and J.C. Polonio, *Biotechnology Research and Innovation*, 3 (2019) 275.
4. N. Ferronato and V. Torretta, *International journal of environmental research and public health*, 16 (2019) 1060.
5. J. Rouhi, C.R. Ooi, S. Mahmud and M.R. Mahmood, *Materials Letters*, 147 (2015) 34.
6. H. Karimi-Maleh, S. Ranjbari, B. Tanhaei, A. Ayati, Y. Orooji, M. Alizadeh, F. Karimi, S. Salmanpour, J. Rouhi and M. Sillanpää, *Environmental Research*, 195 (2021) 110809.
7. E. Brillas and C.A. Martínez-Huitle, *Applied Catalysis B: Environmental*, 166 (2015) 603.
8. J. Rouhi, S. Kakooei, M.C. Ismail, R. Karimzadeh and M.R. Mahmood, *International Journal of Electrochemical Science*, 12 (2017) 9933.
9. T. Puzyn, B. Rasulev, A. Gajewicz, X. Hu, T.P. Dasari, A. Michalkova, H.-M. Hwang, A. Toropov, D. Leszczynska and J. Leszczynski, *Nature nanotechnology*, 6 (2011) 175.
10. B. Gong, P. Wu, J. Yang, X. Peng, H. Deng and G. Yin, *International Journal of Electrochemical Science*, 16 (2021) 21023.
11. T. Tong, J. Zhang, B. Tian, F. Chen and D. He, *Journal of Hazardous Materials*, 155 (2008) 572.
12. M. Huang, C. Xu, Z. Wu, Y. Huang, J. Lin and J. Wu, *Dyes and pigments*, 77 (2008) 327.
13. H. Karimi-Maleh, M. Alizadeh, Y. Orooji, F. Karimi, M. Baghayeri, J. Rouhi, S. Tajik, H. Beitollahi, S. Agarwal and V.K. Gupta, *Industrial & Engineering Chemistry Research*, 60 (2021) 816.
14. R. Hassanzadeh, A. Siabi-Garjan, H. Savaloni and R. Savari, *Materials Research Express*, 6 (2019) 106429.
15. D. Tan, H. Long, H. Zhou, Y. Deng, E. Liu, S. Wang and S. Zhang, *International Journal of Electrochemical Science*, 15 (2020) 12232.
16. Z. Savari, S. Soltanian, A. Noorbakhsh, A. Salimi, M. Najafi and P. Servati, *Sensors and Actuators B: Chemical*, 176 (2013) 335.
17. H. Savaloni, R. Savari and S. Abbasi, *Current Applied Physics*, 18 (2018) 869.
18. H. Karimi-Maleh, M.L. Yola, N. Atar, Y. Orooji, F. Karimi, P.S. Kumar, J. Rouhi and M. Baghayeri, *Journal of colloid and interface science*, 592 (2021) 174.
19. J. Rouhi, S. Kakooei, S.M. Sadeghzadeh, O. Rouhi and R. Karimzadeh, *Journal of Solid State Electrochemistry*, 24 (2020) 1599.
20. J.D.R. Salazar, *Scientia et technica*, 23 (2018) 543.
21. X. Nie, S. Luo, M. Yang, P. Zeng, Z. Qin, W. Yu and Q. Wan, *Minerals*, 9 (2019) 273.
22. X. Pan, M.-Q. Yang, X. Fu, N. Zhang and Y.-J. Xu, *Nanoscale*, 5 (2013) 3601.
23. T.-R. Kuo, H.-J. Liao, Y.-T. Chen, C.-Y. Wei, C.-C. Chang, Y.-C. Chen, Y.-H. Chang, J.-C. Lin, Y.-C. Lee and C.-Y. Wen, *Green Chemistry*, 20 (2018) 1640.
24. C. Mutalik, Y.-C. Hsiao, Y.-H. Chang, D.I. Krisnawati, M. Alimansur, A. Jazidie, M. Nuh, C.-C. Chang, D.-Y. Wang and T.-R. Kuo, *International Journal of Nanomedicine*, 15 (2020) 8911.
25. P. Jubu, F. Yam, V. Igba and K. Beh, *Journal of Solid State Chemistry*, 290 (2020) 121576.
26. J. Li and N. Wu, *Catalysis Science & Technology*, 5 (2015) 1360.
27. L. Li, P.A. Salvador and G.S. Rohrer, *Nanoscale*, 6 (2014) 24.
28. J. Zhi, H. Cui, Z. Wang and F. Huang, *Materials Horizons*, 5 (2018) 691.
29. K.L. Brown, R. Danforth, E. Bleitz, Y. Hwang and D. Rens, *International Journal of Electrochemical Science*, 15 (2020) 10707.

30. P. Rani, A. Ghorai, S. Roy, D.K. Goswami, A. Midya and S.K. Ray, *Materials Research Express*, 6 (2020) 125546.
31. D. Li, H. Song, X. Meng, T. Shen, J. Sun, W. Han and X. Wang, *Nanomaterials*, 10 (2020) 546.
32. K. Kočí, L. Obalová, L. Matějová, D. Plachá, Z. Lacný, J. Jirkovský and O. Šolcová, *Applied Catalysis B: Environmental*, 89 (2009) 494.
33. K. Qi, B. Cheng, J. Yu and W. Ho, *Journal of Alloys and Compounds*, 727 (2017) 792.
34. D.-Y. Wang, C.-H. Li, S.-S. Li, T.-R. Kuo, C.-M. Tsai, T.-R. Chen, Y.-C. Wang, C.-W. Chen and C.-C. Chen, *Scientific reports*, 6 (2016) 1.
35. D. Wojcieszak, M. Mazur, D. Kaczmarek and J. Domaradzki, *Materials Science-Poland*, 35 (2018) 725.
36. V. Etacheri, C. Di Valentin, J. Schneider, D. Bahnemann and S.C. Pillai, *Journal of Photochemistry and Photobiology C: Photochemistry Reviews*, 25 (2015) 1.
37. J. Rashid, S. Saleem, S.U. Awan, A. Iqbal, R. Kumar, M. Barakat, M. Arshad, M. Zaheer, M. Rafique and M. Awad, *RSC advances*, 8 (2018) 11935.
38. L. Yan, X. Yan, H. Li, X. Zhang, M. Wang, S. Fu, G. Zhang, C. Qian, H. Yang and J. Han, *Microchemical Journal*, 157 (2020) 105016.
39. M. Hamadanian, A. Reisi-Vanani and A. Majedi, *Applied Surface Science*, 256 (2010) 1837.
40. S. Hu, A. Wang, X. Li and H. Löwe, *Journal of Physics and Chemistry of Solids*, 71 (2010) 156.
41. H. Tian, J. Ma, K. Li and J. Li, *Ceramics International*, 35 (2009) 1289.
42. L. Deng, S. Wang, D. Liu, B. Zhu, W. Huang, S. Wu and S. Zhang, *Catalysis Letters*, 129 (2009) 13.
43. Z. Wang, L. Shen and S. Zhu, *International Journal of Photoenergy*, 2012 (2012) 1.